ELSEVIER

Journal of Molecular Catalysis A: Chemical 198 (2003) 125–137

JOURNAL OF MOLECULAR CATALYSIS A: CHEMICAL

www.elsevier.com/locate/molcata

Modelling the active sites in vanadyl pyrophosphate

D.J. Thompson [a,*], M.O. Fanning [a], B.K. Hodnett [a,b]

[a] *Department of Chemical and Environmental Sciences, University of Limerick, Limerick, Ireland*
[b] *Materials and Surface Science Institute, University of Limerick, Limerick, Ireland*

Received 27 August 2002; received in revised form 25 October 2002; accepted 28 October 2002

Abstract

The ability of the vanadyl pyrophosphate (1 0 0) surface to selectively activate *n*-butane in the slow step of paraffin oxyfunctionalisation was investigated. Quantum chemical calculations were performed on small cluster models for orthophosphate and pyrophosphate surface terminations. Electrostatic potential surfaces for *n*-butane and the catalyst clusters show favourable electrostatic interaction, with the reactant oriented to maximise Coulombic attraction between terminal hydrogens and surface oxygens. Site-selectivity for covalent interaction at the reactant–surface interface, as measured by frontier molecular orbital (FMO) surfaces and Fukui functions, indicates that surface vanadium species can selectively cleave methylene C–H bonds for butane activation. Both surface terminations, orthophosphate and pyrophosphate, feature the same activation mechanism. The pyrophosphate model, however, has a higher concentration of surface P–O oxygen species which feature prominently in the high-lying occupied orbitals. Hence, the pyrophosphate-terminated surface may promote subsequent controlled oxidation of activated *n*-butane to maleic anhydride. The susceptibility of maleic anhydride to further reaction at the surface was also examined using the active site reactivity analyses.

Keywords: Vanadyl pyrophosphate; Quantum chemical calculations; Cluster models; Fukui functions; *n*-Butane activation

1. Introduction

Vanadyl pyrophosphate $(VO)_2P_2O_7$, is the most selective catalyst for the oxyfunctionalisation of *n*-butane to maleic anhydride [1]. This is the only commercial paraffin oxidation process [2], and in typical industrial plants the maleic anhydride yield is approximately 60%. Significant gains in selectivity and activity for this reaction will only occur if we can understand the system at the molecular level [3]. This is equally true for all mild oxidation reactions [4].

There is still much debate regarding the mode of action of vanadyl pyrophosphate in butane selective oxidation [5]. However, areas of general agreement do exist.

1. The working catalyst is largely composed of $(VO)_2P_2O_7$. The equilibrated VPO catalyst has an average vanadium oxidation state of 4.0–4.04 and a bulk P to V ratio of 1–1.1; the concentration of V^V species decreases close to zero with time on-line [6].
2. The $(VO)_2P_2O_7$ surface derived from the (1 0 0) plane is active for the oxyfunctionalisation of *n*-butane to maleic anhydride [1].
3. The activation of *n*-butane proceeds via irreversible methylene C–H rupture [7].
4. The surface P/V ratio is always between 1.0 and 1.5, in the most selective catalysts [8].

* Corresponding author. Tel.: +353-61-214147.
E-mail address: damien.thompson@ul.ce (D.J. Thompson).

1381-1169/02/$ – see front matter
PII: S1381-1169(02)00594-0

5. At high *n*-butane conversion, the selectivity to maleic anhydride decreases rapidly [9].

Some theoretical studies on the selective oxidation of *n*-butane over vanadyl pyrophosphate have appeared in the literature [10–13], with cluster models used to represent the catalyst (1 0 0) surface. The cluster approximation has been widely applied in studying metal oxide catalysed reactions [14], as it is in tune with the concept of a finite but chemically complex active site.

In the present work, both orthophosphate and pyrophosphate surface terminations are incorporated into active site cluster models. Electronic structures of *n*-butane and maleic anhydride are explicitly considered, as is a dynamic model of reactivity [15]. The dynamic model of reactivity involves electron-deficient and electron-rich, as well as neutral, systems and may be used to predict the extent, direction and site-selectivity of electron transfer at the reactant–surface interface.

2. Methodology and computational details

All calculations were performed using Gaussian98 [16]. Two catalyst cluster models were generated, reflecting the active site of $(VO)_2P_2O_7$ in two different surface terminations. The Open model of the active site involves a surface with P/V equal to that of the bulk, while the Surface Cleft model [8] (hereafter known simply as the Cleft model) corresponds to a surface with P/V equal to 1.5, a typical value measured on industrial catalysts for this reaction [3].

To create surface models, the bulk crystal structure [17] was cleaved along a plane parallel to (1 0 0), breaking PO–P bonds with the $(n-1)$ layer, and PO–P or PO–V bonds with the $(n+1)$ layer for orthophosphate and pyrophosphate termination, respectively. Active site models were then isolated, with hydrogen atoms used to cap dangling bonds.

The resulting Open and Cleft clusters are shown in Fig. 1. The clusters shown in Fig. 1 are quite small; they represent the largest possible clusters for which radical cation and anion structures could be obtained. The applicability of dynamic reactivity indices is limited to modest-sized systems, due to convergence

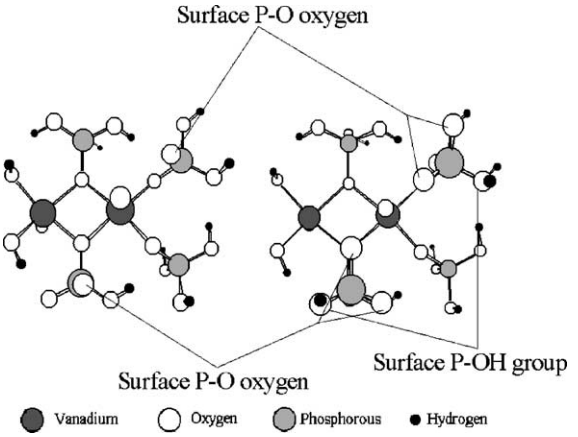

Fig. 1. Open and Cleft models for the vanadyl pyrophosphate active site. A formally neutral Cleft cluster was obtained by capping two surface P–O oxygens with hydrogen; the oxygens labelled "Surface P–O oxygen" in the figure are coordinatively unsaturated in the formally neutral clusters.

problems and hence poorly-equilibrated charge distributions in the radicals.

Electronic structure determinations were performed using the B3LYP [18] functional and 3-21G, 6-31G, and 6-31G* basis sets. Restricted and restricted open-shell calculations describe N_0 and $N_0 + \Delta N$ electron systems, respectively. Mulliken [19]. Natural [20] population analyses were used to compute atomic charges.

A number of reactivity indices [21–24] were used to probe the nature of the active site clusters and substrate molecules, allowing prediction of reaction pathways at the surface. Molecular electrostatic potential (MEP) [21] surfaces were used to predict site-selectivity for charge-controlled (ionic) interactions. For orbital-controlled interaction, site-selectivity may be predicted from comparison of the HOMO in one system, the less electronegative system [15,22], with the LUMO in the other, the basis of frontier molecular orbital (FMO) theory [23]. Fukui functions [24], which allow for orbital relaxation upon global change in electron number, have developed as companion parameters to FMOs. They may be viewed as the dynamic analogue of the HOMO and LUMO, involving explicit consideration of electron-deficient and electron-rich, as well as neutral, systems in determining local reactivity. Recent theoretical work [25] has indicated that it may be possible to obtain Fukui functions from just

the neutral system. The algorithms developed however, are quite novel and have yet to be incorporated into standard molecular modelling packages.

The Fukui function may be defined as the change in electron density at a site r caused by a change in the global number of electrons for the system, see Eq. (1)

$$f(r) = \left(\frac{\partial \rho(r)}{\partial N}\right)_{\nu(r)} \tag{1}$$

where $\nu(r)$ is the external potential. The condition of fixed nuclear geometry arises from a DFT Maxwell relation for $f(r)$ [15].

The electron density as a function of N has a discontinuity of slope at each integral N. By finite-difference, operational formulae may be derived for $f^-(r)$ and $f^+(r)$, and the electron density then condensed to atoms, yielding Eq. (2)

$$\begin{aligned} f^-(r) &= q_{N_0-1}(r) - q_{N_0}(r) \\ f^+(r) &= q_{N_0}(r) - q_{N_0+1}(r) \end{aligned} \tag{2}$$

where $q(r)$ is the charge on atom r. N_0, $N_0 - 1$, and $N_0 + 1$ refer, respectively, to neutral, radical cation, and radical anion systems.

The $f^-(r)$ distribution dictates which sites undergo electrophilic attack by determining each site's ability to donate electron density. Similarly, $f^+(r)$ predicts sites for nucleophilic attack by measuring each site's response to incoming electron density.

Combining this site-specific information with such global reactivity descriptors [22] as absolute hardness and electronegativity, it is clear that a local HSAB theory may be invoked whereby reaction occurs between the hardest atoms in electrostatic interactions and the softest atoms in orbital-controlled (electron transfer) reactions [26]. In orbital-controlled interaction, the reaction sites in a system are places where change in electron density is favourable. Hence, reaction occurs at sites with largest Fukui value. This implies a large change in chemical potential (electronegativity), conducive to minimisation of the grand canonical potential in the post-reaction system [27]. In essence, the Fukui function is a site-specific manifestation of the general principle that electrons flow from regions of low, to high, electronegativity.

3. Results

3.1. Charge-controlled interaction at the butane–$(VO)_2P_2O_7$ interface

Fig. 2 shows MEP surfaces calculated for *n*-butane and the two alternative active site configurations.

Positively-charged hydrogens, terminal hydrogens in the plane of the C–C backbone having the highest positive electrostatic potential, dominate the MEP surface of *n*-butane. The energetically most favourable Coulombic interaction will occur between these hydrogens and the regions of highest negative electrostatic potential at the $(VO)_2P_2O_7$ active surface, the unsaturated P–O oxygens. Orientations of approach of *n*-butane to the surface that maximise this attraction are shown in Fig. 3.

Terminal carbon and terminal hydrogen are the most negative and positive sites, respectively, in *n*-butane, so any ionic interaction with the surface will be propagated principally through these atoms.

3.2. Orbital-controlled interaction at the butane–$(VO)_2P_2O_7$ interface

3.2.1. n-Butane

Once anchored electrostatically at the surface, electron transfer will be initiated by electron donation from *n*-butane to the active site, as predicted by their relative electronegativities; $\chi_{n\text{-butane}} = 2.7\,\text{eV}$, $\chi_{\text{Open}} = 3.8\,\text{eV}$, and $\chi_{\text{Cleft}} = 4.3\,\text{eV}$, as calculated from SCF energies for neutral and radical systems at B3LYP/6-31G*, with the trend insensitive to model chemistry. The absolute electronegativity of a system may be expressed as [15]

$$\chi = \tfrac{1}{2}(I + A), \quad \text{where} \quad I = E_{N_0-1} - E_{N_0} \quad \text{and} \quad A = E_{N_0} - E_{N_0+1} \tag{3}$$

To predict reaction site-selectivity for butane activation, FMO surfaces and Fukui functions are examined, see Fig. 4.

The most nucleophilic carbon in *n*-butane is methylene carbon, as indicated by both the HOMO surface (and corresponding atomic densities, not shown) and f^- distribution. Terminal hydrogen in the plane of the carbon backbone as the local base site, as suggested by its f^- value, is at odds with its relatively low contribution to the HOMO and also its positive

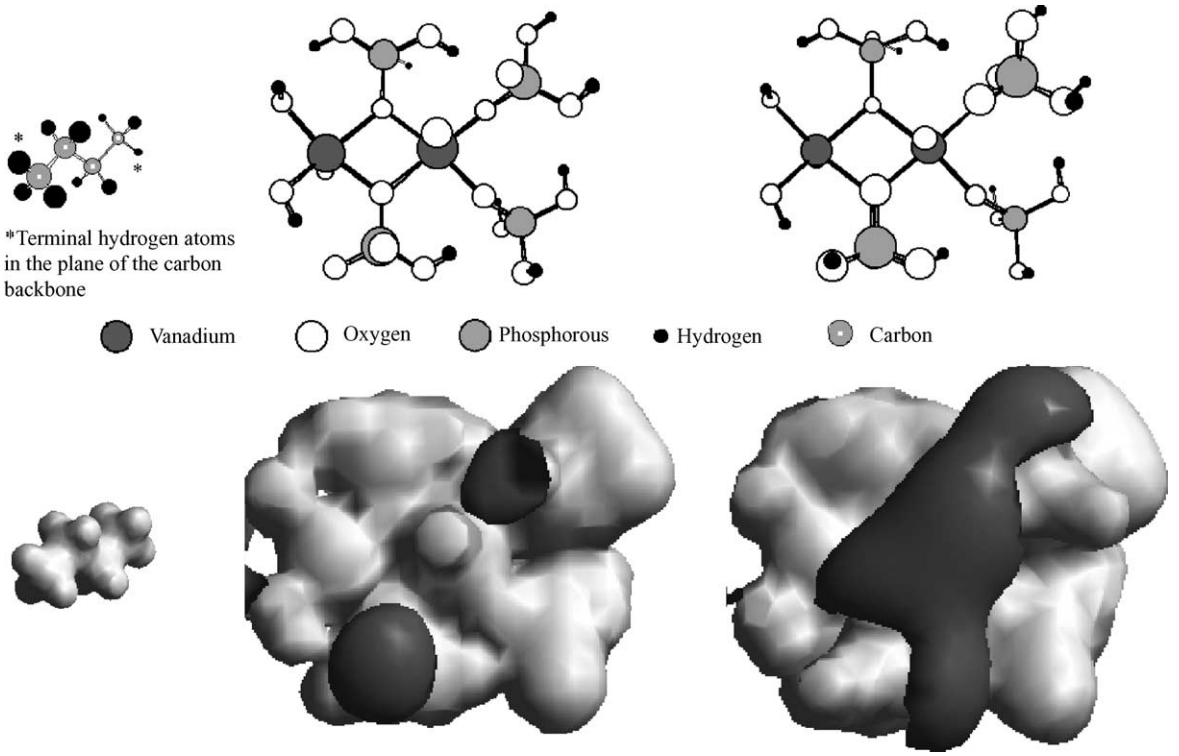

Fig. 2. MEP surfaces for *n*-butane, and Open and Cleft active sites. Isopotential = 3.0 a.u. White and black denote net positive and net negative electrostatic potential, respectively. MEP surfaces are insensitive to model chemistry.

charge. Deconstructing the atomic f^- values to atomic orbital-based functions shows methylene carbon (specifically the $2p_y$ atomic orbital, which forms the methylene C–C bonding combination that predominates the HOMO) to be the site donating the most electron density upon formation of the radical cation, $N_0 - 1$ electron, system.

Hence, we may expect *n*-butane to donate electron density from methylene carbon in its initial covalent interaction with the surface. Of the hydrogens, methylene hydrogen exhibits the most electrophilicity, according to both the LUMO surface and the f^+ distribution.

3.2.2. Open active site

Analysis of local short-range reactivity in the $(VO)_2P_2O_7$ active sites is more complex. Fig. 5 shows FMO wavefunctions calculated for the Open active site.

In-phase and out-of-phase combinations of vanadium $3d_{x^2-y^2}$ atomic orbitals dominate the FMOs, in agreement with recent calculations on a much larger cluster model [13]. Surface P–O oxygens, from which areas of negative electrostatic potential originate (see Fig. 2), do not contribute to the FMOs. Inspection of neighbouring MOs shows, however, that the surface P–O oxygens contribute significantly to high-lying occupied MOs but not low-lying unoccupied MOs.

Fig. 6 shows wavefunctions and cumulative atomic MO densities for the first five occupied MOs in the Open active site.

HOMO-1, HOMO-2, HOMO-3 and HOMO-4 wavefunctions describe surface P–O oxygen lone pair electron orbitals. HOMO-5 and HOMO-6 are significantly lower in energy. They describe the surface P–O bonding oxygen electron and the unpaired oxygen electron for each surface-undersaturated oxygen.

Thus, the static model of local reactivity shows vanadium predominating the HOMO and LUMO, with the neighbouring occupied orbitals built from surface P–O oxygens.

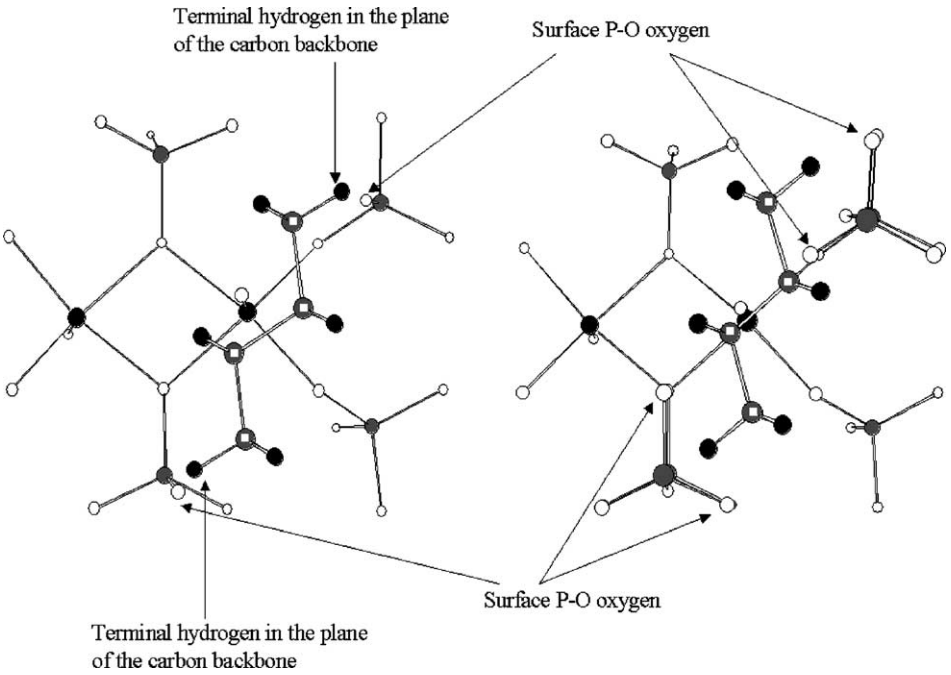

Fig. 3. Electrostatic alignment of *n*-butane at the Open and Cleft active sites. For clarity, atomic display radii are reduced relative to the previous figures (from 25 to 10% the van der Waals radii), and capping Hs are not shown in the clusters.

The identification of vanadium as the local base and acid site in the Open active site is confirmed by Fukui analysis, as shown in Fig. 7.

The deviation with population analysis within a particular basis set is slight; MPA gives practically identical results. The main difference with basis set is in rank orderings for the vanadium atoms and their neighbouring oxygens [28].

3.2.3. *Cleft active site*

Analysis of local reactivity in the Cleft active site also predicts vanadium acting as both the local base

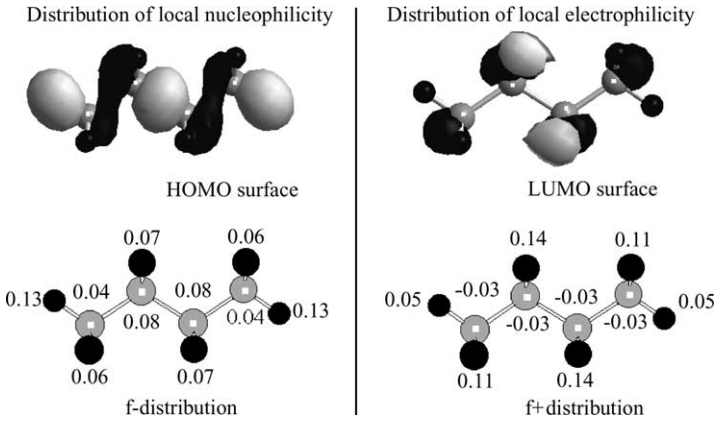

Fig. 4. Local base and local acid sites in *n*-butane. B3LYP/3-21G results shown, with Fukui functions calculated from NPA atomic charges. Rank orderings for atomic FMO densities and Fukui functions are not affected by choice of basis set or method of charge analysis. An isopotential of 0.05 a.u. is used in these, and all subsequent, MO wavefunction plots.

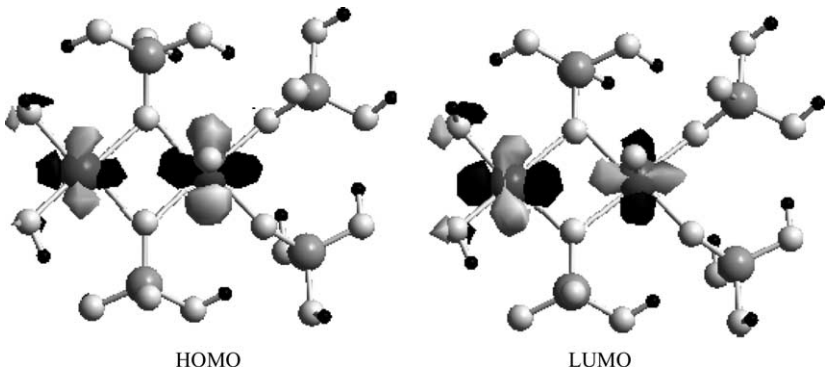

Fig. 5. HOMO and LUMO surfaces for Open active site.

and local acid site, together with strong presence of surface P–O oxygens in the first few occupied orbitals but not in the virtual orbitals. Fig. 8 shows FMO wavefunctions for the Cleft active site, while Fig. 9 shows atomic molecular orbital (MO) densities summed over the first nine occupied MOs, and also the Fukui distributions. The first nine occupied MOs include wavefunctions for vanadium and also for both pairs of p electrons on each surface P–O oxygen. Hence, eight MOs, compared to four for the Open active site, are necessary to describe P–O oxygen non-bonding electron orbitals in the Cleft model; this is because the number of surface P–O oxygens is doubled in the Cleft active site cluster.

The main effect of pyrophosphate termination is a change in ordering of occupied MOs (the bonding combination of vanadium $3d_{x^2-y^2}$ AOs is demoted in energy from HOMO to HOMO-4 upon pyrophosphate termination) and a more significant f^- value on surface P–O oxygens. However, vanadium remains the local base and acid site, according to the dynamic

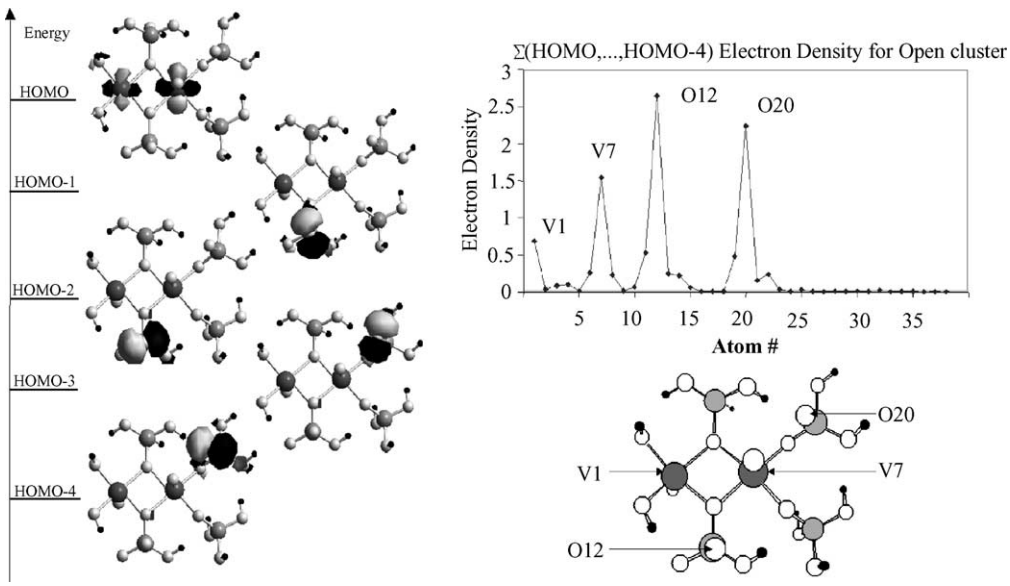

Fig. 6. HOMO-x ($x = 0, \ldots, 4$) surfaces and densities for Open active site. B3LYP/3–21G results used, with larger basis sets giving qualitatively identical results.

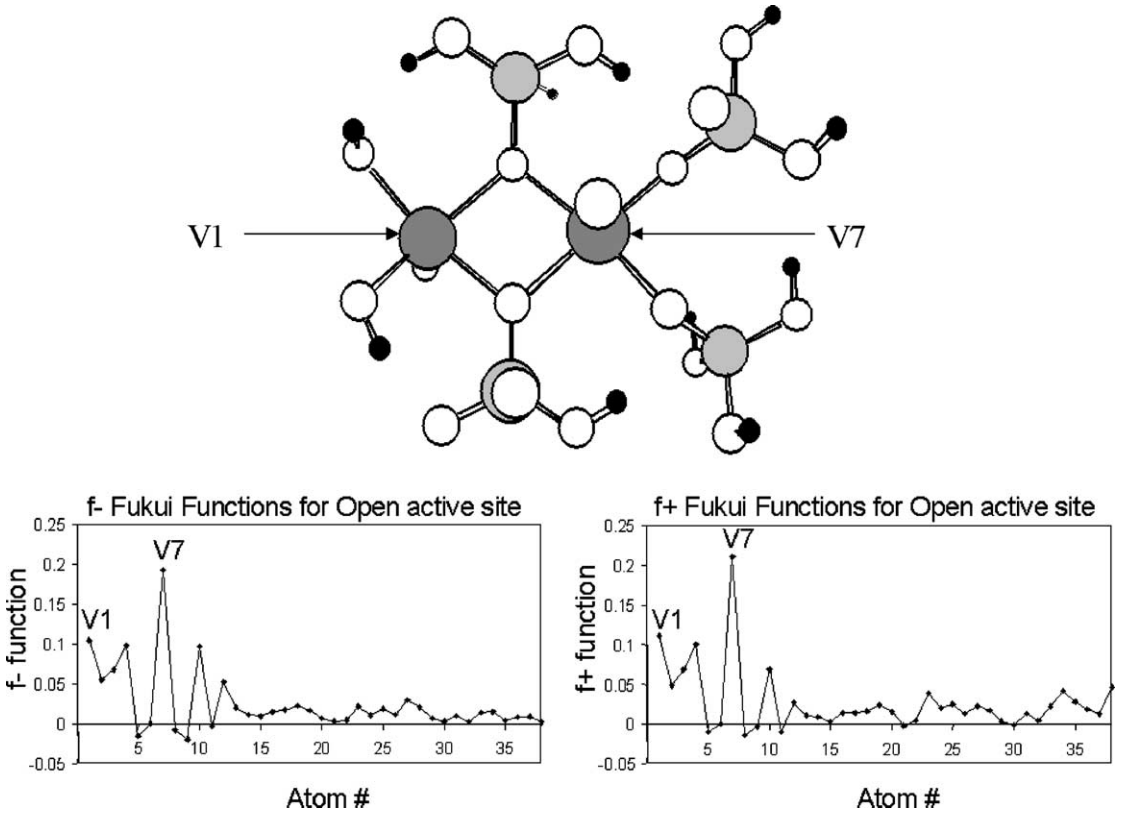

Fig. 7. Fukui analysis for Open active site. B3LYP/3-21G, with NPA, results shown.

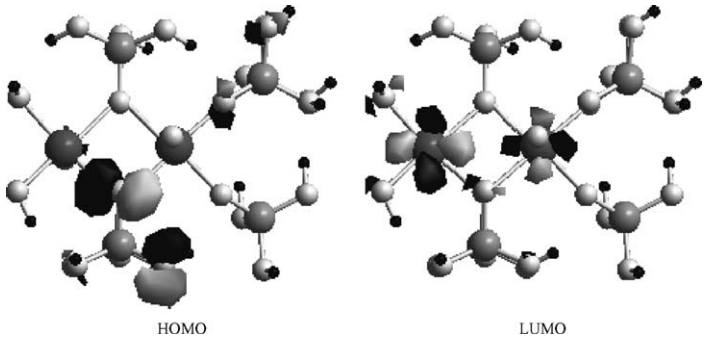

Fig. 8. HOMO and LUMO surfaces for the Cleft active site model.

model of reactivity, when vanadyl pyrophosphate features surface enrichment in phosphorous. Again, detailed analysis of the Fukui distributions is not presented here [28].

Armed with these results, we may construct the energetically most favourable path for *n*-butane covalent interaction with the vanadyl pyrophosphate surface.

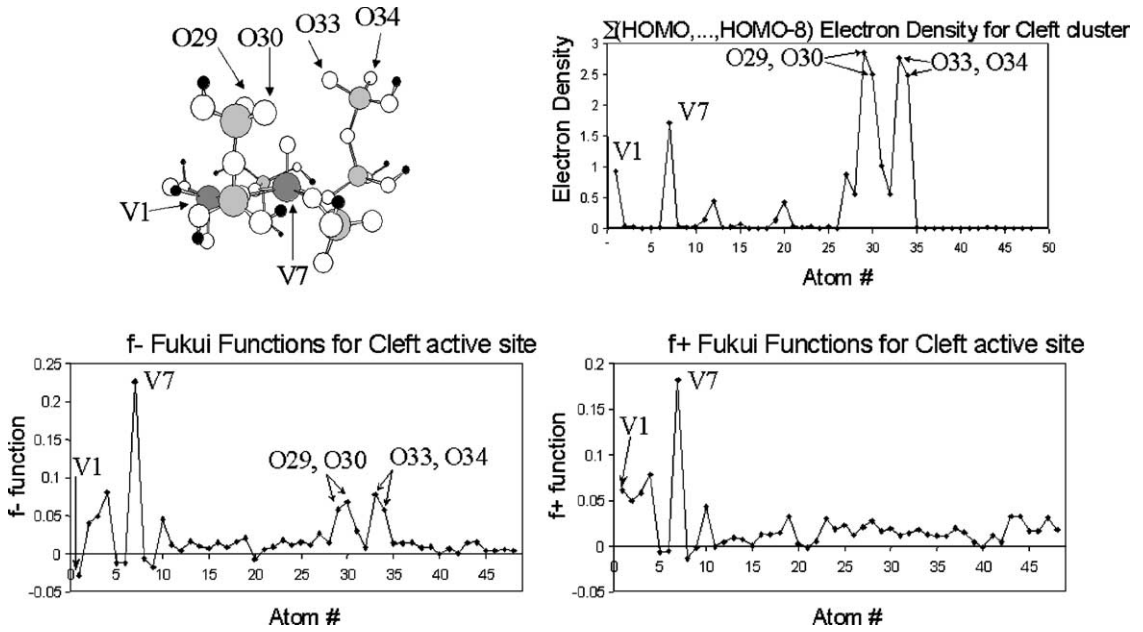

Fig. 9. Atomic constituents of outer-lying occupied orbitals, and Fukui distributions in the Cleft active site. B3LYP/3-21G with NPA results shown. MPA gave similar Fukui distributions, for all basis sets.

4. Discussion

4.1. n-Butane interaction with the $(VO)_2P_2O_7$ surface

4.1.1. Adsorption and activation

Since neither the methylene carbons nor methylene hydrogens carry the highest charges in *n*-butane, the present work indicates that selective activation of *n*-butane is not possible via charge-controlled interaction. Though the global hardness of *n*-butane suggests its participation in ionic interactions [26], this type of interaction will not lead to selective dehydrogenation.

NH_3 (absolute hardness, $\eta = 8.2$ eV [15]) chemisorbs at the vanadyl pyrophosphate surface [29], indicating that hard molecules can interact covalently with the surface. Recent theoretical studies [30] on zeolite catalysis also used short-range reactivity indices to rationalise the interaction of hard molecules such as N_2 ($\eta = 8.9$ eV), CO_2 ($\eta = 7.3$ eV), and CO ($\eta = 7.9$ eV), with a soft ($\eta \sim 3.0$ eV) zeolite active site. Hence, Fukui functions and local softnesses are now used to derive a site-selective mechanism for butane activation.

Once anchored electrostatically at the surface, any covalent interaction will be initiated by flow of electron density from methylene carbon to vanadium, as predicted by global and local reactivity analysis. A side effect of this adsorption is that methylene hydrogen is placed in the vicinity of vanadium, as close as their positive charges will allow. The identification of vanadium as the local base site in the active site is conducive to concomitant electron donation to methylene hydrogen (population of the methylene C–H σ^* contribution to the LUMO, see Fig. 4). Hence, *n*-butane may be attacked by vanadium via a dual acid–base mechanism.

Fig. 10 shows site-selectivity for acid, and acid–base attack, on *n*-butane. The arrows, in this and all subsequent figures, indicate the direction, but not extent, of electron flow; as explained below, the hardness of butane means the interaction is weak.

The net effect of adsorption through methylene carbon and donation of electron density to methylene hydrogen is weakening of methylene C–H bonds, with methylene C–H rupture activating butane at the surface.

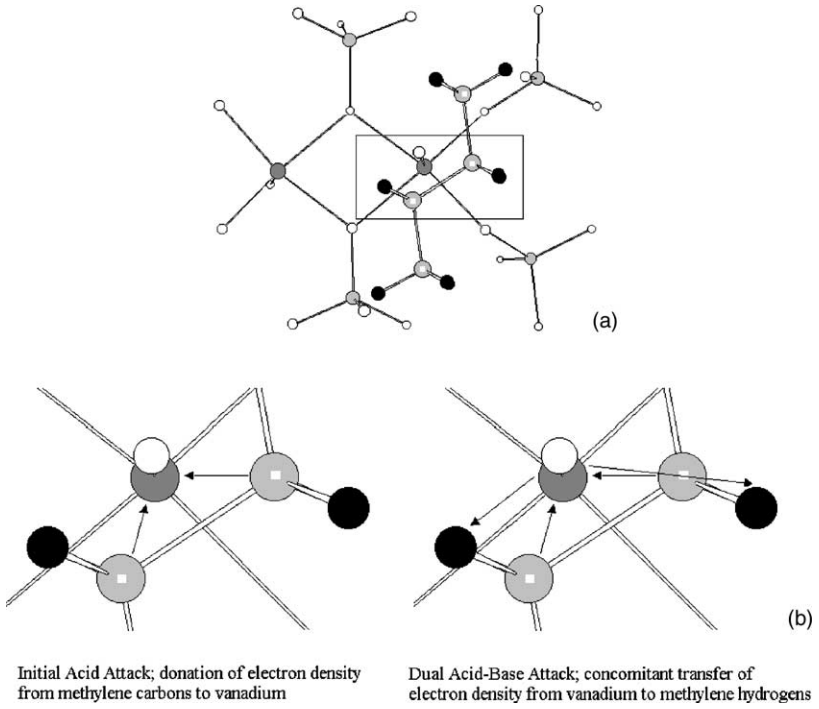

Fig. 10. (a) Electrostatic alignment of butane at the surface; the Cleft active site, not shown, features a similar orientation of approach, see Fig. 3. (b) Acid and acid–base attack on *n*-butane by vanadium at the $(VO)_2P_2O_7$ surface.

Eq. (4) [22] quantifies the number of electrons transferred between species A and B ($\chi_A > \chi_B$) in the initial covalent interaction

$$\Delta N = \frac{\chi_A - \chi_B}{2(\eta_A + \eta_B)} \quad (4)$$

For *n*-butane electron donation to the surface, ΔN is <0.1, due to the high hardness of *n*-butane. The hardness of *n*-butane assists in the dual acid–base activation mechanism. A higher ΔN for the initial interaction would be advantageous to only acid attack at methylene carbon, without base attack at methylene hydrogen, whereby C_2–C_3 cleavage products would predominate.

Analysis of local softness [15] values, Fukui function of the most reactive site times the global softness of the system, shows how vanadium has much higher electron donor/acceptor power than the reaction sites on butane, see Table 1. Global softness [15], the inverse of absolute hardness, is calculated in a similar manner to absolute electronegativity [15], where the operational formula for global softness is

$$S = \frac{2}{I - A} \quad (5)$$

Local softness serves as a measure of intermolecular reactivity, carrying knowledge of both inherent and site-specific reactivity. Vanadium local softness is far greater than that of either the methylene carbon or hydrogen, indicating that vanadium may perform

Table 1
Comparison of electron donor/acceptor powers in *n*-butane and $(VO)_2P_2O_7$ active sites

B3LYP/3-21G	S	f^-	s^-	f^+	s^+
n-Butane	0.07	0.08	0.01	0.14	0.01
Open cluster	0.83	0.19	0.16	0.21	0.17
Cleft cluster	0.76	0.23	0.17	0.18	0.14

3-21G results are used, but trends are insensitive to level of theory. f^- and f^+ for *n*-butane are for methylene carbon and methylene hydrogen, respectively. f^- and f^+ for the active site clusters are for vanadium.

multi-site attack on butane. Hence the concerted 2,3-methylene C–H cleavage activation mechanism shown in Fig. 10, which is also in agreement with previous correlations between calculated and observed rate constants for this reaction [1]. The mismatching of *n*-butane and the active site in terms of relative electron donor/acceptor power suggests a weak interaction [26], in agreement with the observed low rate of butane activation at the surface [31].

A recent IR study [32] has reported strong experimental evidence for *n*-butane activation at vanadium sites, while another very recent study [33] involving the use of isotopically labelled *n*-butane indicated that the non-selective oxidation of *n*-butane involves abstraction of methyl groups; the methylene C–C bond is not ruptured at the surface.

These observations are in agreement with the dual acid–base mechanism proposed above. *n*-Butane is adsorbed via nucleophilic attack of methylene carbon on vanadium, but the methylene C–C bond is not cleaved, because of the weakness of the interaction and the accompanying transfer of electron density from vanadium to methylene hydrogen.

4.1.2. Effect of surface enrichment in phosphorous

Temporal analysis of products (TAP) work [1,34], has led to the proposition of a surface lattice oxygen species, O_{SL}, responsible for allylic oxydehydrogenation of, and oxygen insertion into, activated *n*-butane. Results indicate that selectivity to maleic anhydride is a function of $[O_{SL}]$ at the active site, also in agreement with recent isotope work [33].

Electrophilic oxygen species are generally thought to promote the formation of C–C cleavage, total oxidation, products. Surface radical oxygen, formally $^{\bullet}O$, is generally thought to be an electron acceptor, wanting an extra electron to fill its p-shell [9].

In the analysis of reactive sites on vanadyl pyrophosphate, however, surface P–O oxygen species exhibit only electron donor properties, as seen by their strong contribution to the outer occupied MOs but not to the virtual orbitals. This is confirmed by Fukui analysis, where they show significant basicity (f^- value), particularly in the Cleft cluster, but not acidity (f^+). Neither V–O–V nor V–O–P oxygens show reactivity.

Hence, given that surface P–O oxygens exhibit nucleophilic but not electrophilic properties, they may provide a source of selective oxygen species for C–H rather than C–C cleavage in post-activation steps. This may explain why surface enrichment in phosphorous is necessary for more selective vanadyl pyrophosphate catalysts, since a phosphorous-enriched surface naturally features more P–O oxygen species.

4.1.3. Maleic anhydride interaction with the $(VO)_2P_2O_7$ surface

Maleic anhydride, the selective oxidation product, is more electronegative than either type of vanadyl pyrophosphate active site; $\chi_{\text{maleic anhydride}} = 6.1\,\text{eV}$ at B3LYP/6-31G*. Regardless of model chemistry, maleic anhydride is always more electronegative than the clusters.

Hence, any covalent interaction will proceed via base attack by the surface on acid sites in maleic anhydride. Fig. 11 shows the MEP surface of maleic anhydride, the electrostatics involved in maleic anhydride's approach to the surface, local base and acid sites in maleic anhydride, and a possible mode of activation.

The MEP surface for maleic anhydride shows positive charge over all atoms except oxygens. Hence, the π electron density of the C=C carbons appears to be drowned out by the neighbouring positive C=O carbons and =C–H hydrogens, meaning the C=C carbons are contained within a positive electrostatic field. MEP-based atomic charges for organic molecules, whose signs are counterintuitive but explain observed phenomena better than atomic charges computed from standard population analyses, have been presented in earlier studies [35]. As for the identification of C=C carbons as the local acid sites, previous theoretical studies [36] on the reactivity of α, β unsaturated systems containing carbonyl and olefin groups showed how the complexity arising from α, β unsaturation causes the C=C carbons to show high electrophilicity as the resultant negative charge, upon charge acceptance from a nucleophile, is distributed by delocalisation.

Hence, electron donation from surface P–O oxygens and vanadium to the C=C carbons may initiate covalent chemisorption.

If however, the orientation of maleic anhydride is as shown in Fig. 11(b)(ii), with the olefin carbons pointing away from the surface, the local acid site in the substrate is shielded from surface base sites. The electronegativity gradient precludes electron transfer from

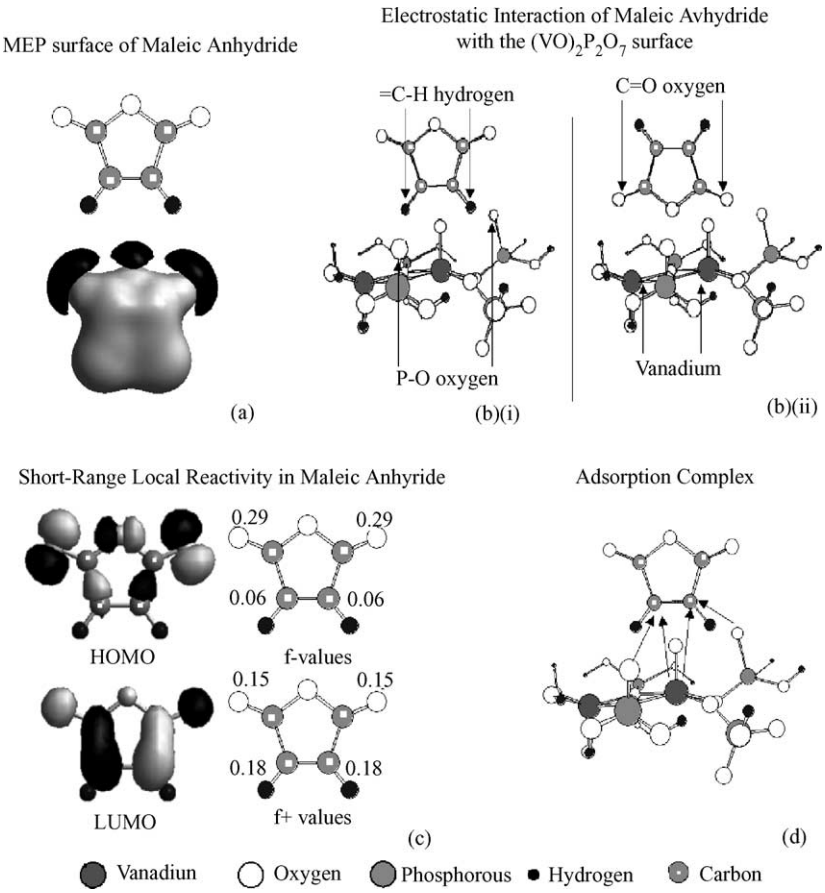

Fig. 11. (a) MEP surface of maleic anhydride. (b) Two alternative orientations for electrostatic alignment of maleic anhydride at the Open active site. =C–H hydrogens and C=O oxygens are the sites of highest positive and negative charge, respectively, in maleic anhydride. The Cleft active site (not shown) can also feature either orientation of approach. (c) Local nucleophilicity (HOMO and f^- values) and electrophilicity (LUMO and f^+ values) in maleic anhydride. B3LYP/3–21G with NPA results shown. Only highest values shown. (d) Chemisorption of maleic anhydride at the $(VO)_2P_2O_7$ surface. Open active site shown, but mechanism can operate with either surface termination.

carbonyl oxygen (the local base site in maleic anhydride) to vanadium. Carbonyl oxygens, the only other sites exhibiting significant acidity in maleic anhydride, are exposed to the surface but electron donation to a region of negative electrostatic potential is unlikely to initiate covalent bonding.

This orientation is what results from a chelating mechanism [33] for butane oxidation by the surface. Hence, maleic anhydride, once formed in the active site, will not be further transformed. If, however, it subsequently re-approaches the surface, maleic anhydride may be re-adsorbed in an orientation which permits its degradation, regardless of surface termination.

So, while the vanadyl pyrophosphate surface can selectively activate butane and, with sufficient selective oxygen species, form maleic anhydride, high levels of conversion are undesirable due to the vulnerability of the selective oxidation product to further transformation.

5. Conclusions

The mode of action of the vanadyl pyrophosphate surface in catalysing the selective oxidation of *n*-butane to maleic anhydride was investigated using

small cluster models for the catalyst active surface. Molecular electrostatic potential surfaces, absolute hardness and electronegativity values, frontier molecular orbital (and neighbouring orbital) surfaces, Fukui functions, and local softnesses were calculated for *n*-butane, maleic anhydride, and two distinct active site models, and then used to propose mechanisms for substrate–surface interaction.

The overall conclusion is that vanadium is responsible for adsorption and activation of *n*-butane at the $(VO)_2P_2O_7$ surface. Both vanadium and surface P–O oxygens participate in the further transformation of maleic anhydride at the surface.

Surface-unsaturated P–O oxygens may aid in electrostatic docking of butane at the surface and also provide a source of selective oxygen species for the further transformation of activated butane to more functionalised, and hence more valuable, products. Therefore, surface termination is critical in optimising selectivity since a pyrophosphate-terminated surface naturally features a greater concentration of such species.

The main limitation of the present work is that the vanadyl pyrophosphate surface is modelled using finite clusters with bulk geometry. Hence, ab initio calculations on the extended, relaxed surface are necessary to gain further insight into the reaction mechanism at work in *n*-butane's oxyfunctionalisation over vanadyl pyrophosphate. This work is in progress.

Acknowledgements

Professor Rutger van Santen is thanked for helpful discussions during the course of this work.

References

[1] G. Centi, F. Trifiro, J.R. Ebner, V.M. Franchetti, Chem. Rev. 88 (1988) 55.
[2] J.C. Volta, Comptes Rendus de l'Academie des Sciences–Serie IIC–Chimie 3 (2000) 717.
[3] G. Centi, Catal. Today 16 (1993) 1.
[4] C.R.A. Catlow, J.B. Nicholas, R.A. van Santen, Top. Catal. 9 (1999).
[5] B.K. Hodnett, Heterogeneous Catalytic Oxidation: Fundamental and Technological Aspects of the Selective and Total Oxidation of Organic Compounds, Wiley, New York, 2000.
[6] G. Centi, F. Trifiro, G. Busca, J. Ebner, J. Gleaves, Faraday Discuss. Chem. Soc. 87 (1989) 215.
[7] M.A. Pepera, J.L. Callahan, M.J. Desmond, E.C. Milberger, P.R. Blum, N.J. Bremer, J. Am. Chem. Soc. 107 (1985) 4883.
[8] J.R. Ebner, M.R. Thompson, Catal. Today 16 (1993) 51.
[9] F.E. Cassidy, Ph.D. Thesis, University of Limerick, 1999.
[10] J. Ziolkowski, E. Bordes, P. Courtine, J. Catal. 122 (1990) 126.
[11] B. Schiott, K.A. Jorgensen, R. Hoffmann, J. Phys. Chem. 95 (1991) 2297.
[12] J. Haber, R. Tokarz, M. Witko, Heterogenous Hydrocarbon Oxidation 638 (1996) 249.
[13] M. Witko, R. Tokarz, J. Haber, K. Hermann, J. Mol. Catal. A: Chem. 166 (2001) 59.
[14] (a) W. Langenaeker, N. Coussement, F. De Proft, P. Geerlings, J. Phys. Chem. 98 (1994) 3010;
(b) N.U. Zhanpeisov, M. Matsuoka, H. Mishima, H. Yamashita, M. Anpo, J. Mol. Struct. (Theochem.) 454 (1998) 201;
(c) I.V. Yudanov, P. Gisdakis, C. Di Valentin, N. Rosch, Eur. J. Inorg. Chem. 10 (1999) 2135;
(d) K.M. Neyman, S. Vent, N. Rosch, G. Pacchioni, Top. Catal. 9 (1999) 153.
[15] R.G. Parr, W. Yang, Density-Functional Theory of Atoms and Molecules, Oxford University Press, Oxford, 1989.
[16] Gaussian98, Revision A.8, M.J. Frisch, G.W. Trucks, H.B. Schlegel, G.E. Scuseria, M.A. Robb, J.R. Cheeseman, V.G. Zakrzewski, J.A. Montgomery Jr., R.E. Stratmann, J.C. Burant, S. Dapprich, J.M. Millam, A.D. Daniels, K.N. Kudin, M.C. Strain, O. Farkas, J. Tomasi, V. Barone, M. Cossi, R. Cammi, B. Mennucci, C. Pomelli, C. Adamo, S. Clifford, J. Ochterski, G.A. Petersson, P.Y. Ayala, Q. Cui, K. Morokuma, D.K. Malick, A.D. Rabuck, K. Raghavachari, J.B. Foresman, J. Cioslowski, J.V. Ortiz, A.G. Baboul, B.B. Stefanov, G. Liu, A. Liashenko, P. Piskorz, I. Komaromi, R. Gomperts, R.L. Martin, D.J. Fox, T. Keith, M.A. Al-Laham, C.Y. Peng, A. Nanayakkara, M. Challacombe, P.M. W. Gill, B. Johnson, W. Chen, M.W. Wong, J.L. Andres, C. Gonzalez, M. Head-Gordon, E.S. Replogle, J.A. Pople, Gaussian Inc., Pittsburgh, PA, 1998.
[17] Y.E. Gorbunova, S.A. Linde, Sov. Phys. Dokl. 24 (1979) 138.
[18] A.D. Becke, J. Chem. Phys. 98 (1993) 5648.
[19] R.S. Mulliken, J. Chem. Phys. 32 (1962) 3428.
[20] A.E. Reed, R.B. Weinstock, F. Weinhold, J. Chem. Phys. 83 (1985) 735.
[21] A. Hinchliffe, Modelling Molecular Structures, Wiley, 1997.
[22] R.G. Parr, R.G. Pearson, J. Am. Chem. Soc. 105 (1983) 7512.
[23] K. Fukui, Theory of Orientation and Stereoselection: Reactivity and Structure Concepts in Organic Chemistry, vol. 2, Springer, Berlin, 1973.
[24] R.G. Parr, W. Yang, J. Am. Chem. Soc. 106 (1984) 4049.
[25] (a) A. Michalak, F. De Proft, P. Geerlings, R.F. Nalewajski, J. Phys. Chem. A 103 (1999) 762;
(b) R. Contreras, P. Fuentealba, M. Galvan, P. Perez, Chem. Phys. Lett. 304 (1999) 405;
(c) P. Fuentealba, P. Perez, R. Contreras, J. Chem. Phys. 113 (2000) 2544.

[26] P.K. Chattaraj, J. Phys. Chem. A 105 (2001) 511.
[27] P.W. Ayers, R.G. Parr, J. Am. Chem. Soc. 122 (2000) 2010.
[28] D.J. Thompson, Ph.D. Thesis, University of Limerick, 2003.
[29] G. Busca, G. Centi, F. Trifiro, V. Lorenzelli, J. Phys. Chem. 90 (1986) 1337.
[30] S. Pal, K.R.S. Chandrakumar, J. Am. Chem. Soc. 122 (2000) 4145.
[31] F. Cavani, F. Trifiro, Chemtech 24 (1994) 18.
[32] G. Koyano, T. Saito, M. Misono, J. Mol. Catal. A: Chem. 155 (2000) 31.
[33] B. Chen, E.J. Munson, J. Am. Chem. Soc. 124 (2002) 1638.
[34] J.T. Gleaves, G. Centi, Catal. Today 16 (1993) 69.
[35] G. Busca, E. Finocchio, G. Ramis, G. Ricchiardi, Catal. Today 32 (1996) 133.
[36] R.K. Roy, S. Krishnamurti, P. Geerlings, S. Pal, J. Phys. Chem. A 102 (1998) 3746.